Spherical beampatterns with fractional orders

Thibaut Carpentier

forum acusticum 2023

SPHERICAL BEAMPATTERNS WITH FRACTIONAL ORDERS

Thibaut Carpentier
STMS, IRCAM – CNRS – Sorbonne Université – Ministère de la Culture, Paris, France
thibaut.carpentier@ircam.fr

ABSTRACT

Three-dimensional beampatterns can be flexibly and efficiently designed in the spherical harmonics domain. This has a number of useful applications such as beamforming the signals received by spherical microphone arrays, or controlling radiating sound beams produced by compact spherical loudspeaker arrays. However, with the existing design methods, the beampattern orders are restricted to integer numbers. In this paper, we present an approach to the design of axis-symmetric spherical beampatterns with fractional orders. This is typically useful in audio applications where smooth user control is desirable.

First, we derive an analytical expression of the fractional-order beamforming weights, so that the beampattern matches a design objective such as a target directivity index. Then, we present an example of spherical hyper-cardioid pattern (for which the analytical solution is particularly concise) which effectively achieves continuously adjustable directivity index. Our results are in line with a similar study previously published by Huang et al. (2018), yet our approach is both simpler and more generic. As another novel contribution, we extend the method to fractional-order cardioid, super-cardioid, and max-r_E beampatterns.

Keywords: spherical beamforming, directivity index, microphone arrays, maximum front-back ratio.

1. INTRODUCTION

Three-dimensional beampatterns can be conveniently expressed in the spherical harmonics domain, with typical applications in the design of beamforming algorithms for differential microphone arrays [1–4]. Given the hierarchical structure of the spherical harmonic functions, the produced directivity pattern depends on an integer order N, and its shape follows a N-th order trigonometric polynomial in the angle of incidence. The coefficients of this polynomial have to be determined according to some (physically meaningful) objective criterion, such as directivity factor or front-back ratio; this has been extensively studied in the literature [1–8]. Beamformers with high order N can achieve a high directivity factor, however at the expense of robustness issues (higher sensibility to noise and uncertainties). There is therefore a need for highly flexible design strategies. One generalized design framework was proposed [9, 10] in order to generate beampatterns with a combination of criteria (a front-back energy ratio and a smoothness term). Alternatively, beamformers with fractional order have been recently introduced [11, 12], in the context of beamforming with differential microphone arrays, typically to offer an improved trade-off between directivity factor and white noise gain criteria. More generally, fractional order designs can offer a user-friendly way to continuously transition between the omnidirectional pattern and the pattern corresponding to the maximum order N. This has potential applications in audio applications where smooth variation of the beampattern characteristics is desired, for instance for artistic control of radiation synthesis with spherical loudspeaker arrays [13]. In this article, we extend an approach, previously proposed for 3D hyper-cardioid patterns [11] and for planar beamformers [12], that consists in interpolating between patterns of orders N and $N-1$. We show how to determine analytically the proper fractional order for a given target beampattern. We examine several canonical beampatterns, such as hyper-cardioid, super-cardioid, and so-called *in-phase* and max-r_E.

2. DESIGN OF BEAMPATTERNS WITH FRACTIONAL ORDERS

Axis-symmetric spherical beampatterns can be efficiently represented in the spherical harmonics domain [1, 3, 4]: the (frequency-independent) beampattern, with finite or-

der N, writes (Eqn. 5.24 in [4])

$$\mathcal{Y}_N(\Theta) = \sum_{n=0}^{N} d_{N,n} \frac{2n+1}{4\pi} \mathcal{P}_n(\cos\Theta) \ , \qquad (1)$$

where Θ is the angle between the observed and steered directions, and $\mathcal{P}_n(\cdot)$ is the Legendre polynomial of order n. The array weighting factors $d_{N,n}$ are real coefficients which determine the shape of the directivity pattern.

We wish to design a beampattern generalized for arbitrary order $\nu \in \mathbb{R}$, i.e. not restricted to discrete orders $n \in \mathbb{N}$. Our aim is to derive the weights $d_{\nu,n}$ for the fractional-order beampattern $\mathcal{Y}_\nu(\Theta)$. We propose a simple model where, for $(N-1) \leq \nu \leq N$, we interpolate between patterns of orders $(N-1)$ and N

$$\mathcal{Y}_\nu = \alpha\, \mathcal{Y}_N + (1-\alpha)\, \mathcal{Y}_{N-1} \ , \qquad (2)$$

where $0 \leq \alpha \leq 1$ denotes the interpolation factor or "tuning parameter". This leads to the following weights

$$d_{\nu,n} = \begin{cases} \alpha\, d_{N,n} + (1-\alpha)\, d_{N-1,n} & \text{if } 0 \leq n < N \\ \alpha\, d_{N,n} & \text{if } n = N \ . \end{cases} \qquad (3)$$

The aim of this work is to determine the appropriate value of α, as a function of the desired fractional order ν. In order to uniquely estimate α, a given constraint criterion will be further imposed.

3. FRACTIONAL-ORDER BEAMPATTERNS WITH A SPECIFIED DIRECTIVITY INDEX

3.1 Directivity index

The directivity factor quantifies the ratio between the magnitude of the beam pattern in the look direction and the magnitude averaged over all directions. For the axis-symmetric beampattern in Eqn. (1), the directivity factor writes (see Eqn. 5.30 in [4])

$$\mathcal{DF}_N = \frac{\left| \sum_{n=0}^{N} d_{N,n} \frac{2n+1}{4\pi} \right|^2}{\frac{1}{4\pi} \sum_{n=0}^{N} |d_{N,n}|^2 \frac{2n+1}{4\pi}} \ ,$$

and the directivity index is defined such as

$$\mathcal{DI}_N = 10 \log_{10} \mathcal{DF}_N \ .$$

3.2 Derivation of the fractional order

In this section, we express the directivity factor of the fractional-order beampattern $\mathcal{DF}_\nu$ as a function of α. To do so, we introduce two helper variables χ_ν and ψ_ν such that $\mathcal{DF}_\nu = |\chi_\nu|^2 / \psi_\nu$ with

$$\begin{cases} \chi_\nu = \sum_{n=0}^{N} d_{\nu,n} \frac{2n+1}{4\pi} \ , \\ \psi_\nu = \frac{1}{4\pi} \sum_{n=0}^{N} |d_{N,n}|^2 \frac{2n+1}{4\pi} \ . \end{cases}$$

Let's further expand these two helper variables, starting with χ_ν

$$\chi_\nu = \sum_{n=0}^{N} d_{\nu,n} \frac{2n+1}{4\pi} = \sum_{n=0}^{N-1} d_{\nu,n} \frac{2n+1}{4\pi} + d_{\nu,N} \frac{2N+1}{4\pi} \ ,$$

which, after inserting Eqn. (3), reduces to

$$\chi_\nu = \alpha\, \chi_N + (1-\alpha)\, \chi_{N-1} \ .$$

It follows that $|\chi_\nu|^2$ is a second order polynomial in α

$$\begin{aligned} |\chi_\nu|^2 &= \alpha^2\, \chi_N^2 + (1-\alpha)^2\, \chi_{N-1}^2 + 2\,\alpha\,(1-\alpha) \chi_N\, \chi_{N-1} \\ &= \alpha^2\, R + \alpha\, S + T \ , \end{aligned}$$

with

$$\begin{cases} R = \chi_N^2 + \chi_{N-1}^2 - 2\, \chi_N\, \chi_{N-1} \ , \\ S = 2\, (\chi_N\, \chi_{N-1} - \chi_{N-1}^2) \ , \\ T = \chi_{N-1}^2 \ . \end{cases}$$

The variables R, S, and T obviously depend on N, but the subscript index is omitted for the sake of notational simplicity.

Following a similar strategy with the helper variable ψ_ν

$$\begin{aligned} \psi_\nu &= \frac{1}{4\pi} \sum_{n=0}^{N-1} |d_{N,n}|^2 \frac{2n+1}{4\pi} + \frac{1}{4\pi} |d_{N,N}|^2 \frac{2N+1}{4\pi} \\ &= \alpha^2\, \psi_N + (1-\alpha)^2\, \psi_{N-1} + \alpha\,(1-\alpha)\, \xi_N \ , \end{aligned}$$

with

$$\xi_N = \frac{1}{4\pi} \sum_{n=0}^{N-1} 2\, d_{N,n}\, d_{N-1,n} \frac{2n+1}{4\pi} \ .$$

Again, ψ_ν appears as a second order polynomial in α

$$\psi_\nu = \alpha^2\, U + \alpha\, V + W \ ,$$

where

$$U = \psi_N + \psi_{N-1} - \xi_N \ , \ V = \xi_N - 2\,\psi_{N-1} \ , \ W = \psi_{N-1} \ .$$

We can now write the directivity factor as a function of α

$$\mathcal{DF}_\nu = \frac{|\chi_\nu|^2}{\psi_\nu} = \frac{\alpha^2\, R + \alpha\, S + T}{\alpha^2\, U + \alpha\, V + W} \ . \qquad (4)$$

This second order equation is trivially solved with

$$\alpha = \frac{-B \pm \sqrt{B^2 - 4\,A\,C}}{2\,A}\ ,$$

where we noted

$$A = \mathcal{DF}_\nu\ U - R\,,\quad B = \mathcal{DF}_\nu\ V - S\,,\quad C = \mathcal{DF}_\nu\ W - T\,.$$

Assuming that the weights $d_{N,n}$ are known, and the directivity factor $\mathcal{DF}_\nu$ is imposed to a (valid) value, we can evaluate all the helper variables and analytically determine α, keeping only the solution that satisfies $0 \leq \alpha \leq 1$. Observing Eqn. (4), it is trivial to verify that the boundary conditions are consistent with the discrete-order case

$$\begin{cases} \alpha = 0 \implies \mathcal{DF}_\nu = \frac{T}{W} = \frac{\chi^2_{N-1}}{\psi_{N-1}} = \mathcal{DF}_{N-1}\ , \\ \alpha = 1 \implies \mathcal{DF}_\nu = \frac{R+S+T}{U+V+W} = \frac{\chi^2_N}{\psi_N} = \mathcal{DF}_N\ . \end{cases}$$

4. HYPER-CARDIOID PATTERN

4.1 Discrete-order hyper-cardioid pattern

The maximum directivity factor is achieved by a beampattern referred to as hyper-cardioid [1, 3, 4, 7], and given by the weights (Eqn. 6.10 in [4])

$$\forall n \leq N,\ d_{N,n} = \frac{4\pi}{(N+1)^2}\ . \tag{5}$$

It is easy to show that the corresponding directivity factor obeys (Eqn. 6.11 in [4])

$$\mathcal{DF}_N = (N+1)^2\ . \tag{6}$$

The resulting directivity index $\mathcal{DI}_N$ is presented in Fig. 1 for $N \leq 10$.

4.2 Fractional-order hyper-cardioid pattern

Generalizing Eqn. (6) for the fractional-order beampattern we impose the following constraint on the directivity factor (see solid curve in Fig. 1)

$$\mathcal{DF}_\nu = (\nu+1)^2\ . \tag{7}$$

Substituting Eqn. (5) and Eqn. (7) into the expressions from the previous section, we can straightforwardly evaluate all the necessary helper variables

$$\chi_N = \chi_{N-1} = 1\ ,\quad \psi_N = \frac{1}{(N+1)^2}\ ,\quad \xi_N = \frac{2}{(N+1)^2}$$
$$W = \psi_{N-1} = \frac{1}{N^2}\ ,\quad U = \frac{1}{N^2} - \frac{1}{(N+1)^2}$$
$$R = S = 0\ ,\quad T = 1\ ,\quad V = -2\,U\ ,$$

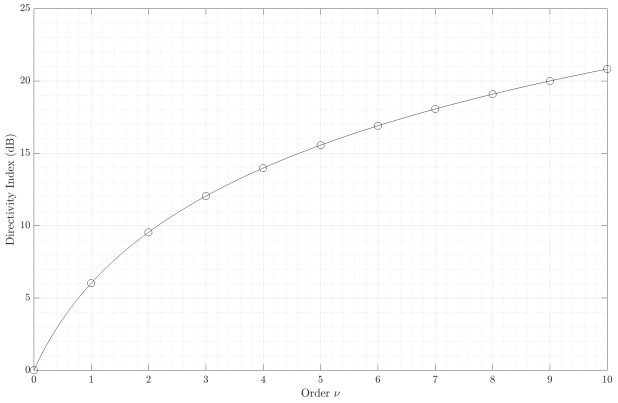

Figure 1: Directivity index of the hyper-cardioid beampattern. Circle markers denote integer orders n; solid curve is for fractional-order ν.

and we derive the following analytic expression for α

$$\alpha = 1 - \frac{N}{\nu+1}\sqrt{\frac{(N-\nu)\,(N+\nu+2)}{2N+1}}\ .$$

This is similar to the result obtained in [11], although with slight differences in notations. The resulting beampattern $\mathcal{Y}_\nu\,(\Theta)$ is presented in Fig. 2 for various values of ν.

5. SUPER-CARDIOID PATTERN

5.1 Discrete-order super-cardioid pattern

While hyper-cardioid patterns maximize the directivity factor, super-cardioid patterns are designed so as to maximize the ratio between the front and back parts of the beam pattern [2, 4]. For a N-th order beampattern, the measure for the front-back ratio can be written as (Eqn. 6.52 in [4])

$$\mathcal{F}_N = \frac{\mathbf{d}_N^H\ \mathbf{A}\ \mathbf{d}_N}{\mathbf{d}_N^H\ \mathbf{B}\ \mathbf{d}_N}\ ,$$

where $\mathbf{d}_N = \left[d_{N,0},\, d_{N,1},\, \ldots\, d_{N,N}\right]^T$ is the vector of beampattern weights, and $\mathbf{A}$ and $\mathbf{B}$ are real, symmetric and positive definite matrices whose elements are related to the coefficients of the Legendre polynomials, and analytically available in equations (6.50) and (6.53) in [4].

5.2 Fractional-order super-cardioid pattern

The front-back ratio $\mathcal{F}_N$ is displayed in Fig. 3 for various values of N. As this does not seem to follow a simple

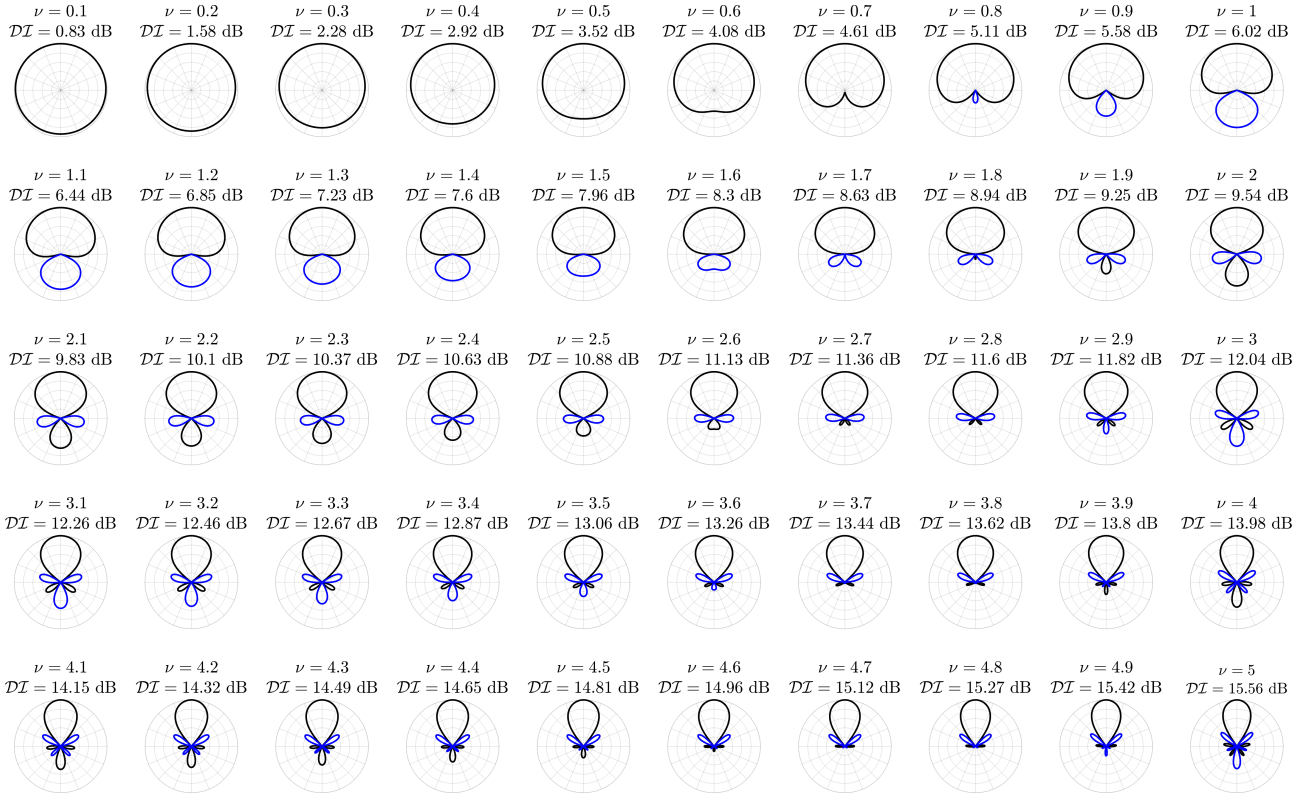

Figure 2: Fractional-order hyper-cardioid beampattern (the radial scale is logarithmic, with 6 dB/division).

closed-form expression, we chose to approximate it with the following polynomial fit (see solid curve in Fig. 3)

$$10 \log_{10} \mathcal{F}_\nu \approx -0.0215\ \nu^3 + 0.473\ \nu^2 + 11.412\ \nu\ ,$$

where $\mathcal{F}_\nu$ denotes the fractional-order front-back ratio

$$\mathcal{F}_\nu = \frac{\mathbf{d}_\nu^H\ \mathbf{A}\ \mathbf{d}_\nu}{\mathbf{d}_\nu^H\ \mathbf{B}\ \mathbf{d}_\nu} = \frac{\mathcal{F}_\nu^{\mathrm{NUM}}}{\mathcal{F}_\nu^{\mathrm{DEN}}}\ ,$$

that we try to express as a function of α. Let's first develop the product $\mathbf{A}\ \mathbf{d}_\nu$, given by

$$\forall n' \in \left[0\ ,N\right]\ ,\ \left[\mathbf{A}\ \mathbf{d}_\nu\right]_{n'} = \sum_{n=0}^{N} d_{\nu,n}\ A_{n,n'}\ .$$

Splitting the sum from 0 to N as

$$\left[\mathbf{A}\ \mathbf{d}_\nu\right]_{n'} = \sum_{n=0}^{N-1} d_{\nu,n}\ A_{n,n'}\ +\ d_{\nu,N}\ A_{N,n'}\ ,$$

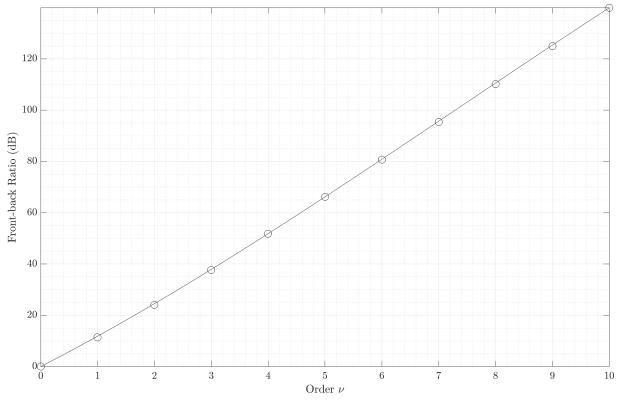

Figure 3: Front-back ratio of the super-cardioid beampattern. Circle markers denote integer orders n; solid curve is for fractional-order ν.

it follows that

$$\left[\mathbf{A}\,\mathbf{d}_\nu\right]_{n'} = \alpha \sum_{n=0}^{N} d_{N,n}\, A_{n,n'} + (1-\alpha) \sum_{n=0}^{N-1} d_{N-1,n}\, A_{n,n'} \ .$$

Introducing this result into $\mathcal{F}_\nu^{\mathrm{NUM}}$, it becomes

$$\begin{aligned}\mathcal{F}_\nu^{\mathrm{NUM}} &= \sum_{n'=0}^{N} d_{\nu,n'} \left[\mathbf{A}\,\mathbf{d}_\nu\right]_{n'} \\ &= \alpha \sum_{n'=0}^{N} d_{N,n'} \left[\mathbf{A}\,\mathbf{d}_\nu\right]_{n'} \\ &\quad + (1-\alpha) \sum_{n'=0}^{N-1} d_{N-1,n'} \left[\mathbf{A}\,\mathbf{d}_\nu\right]_{n'} \ ,\end{aligned}$$

and after some basic developments, we show that

$$\mathcal{F}_\nu^{\mathrm{NUM}} = \alpha^2 \left(D1 - 2D2 + D3\right) + 2\alpha \left(D2 - D3\right) + D3 \,,$$

with

$$\begin{cases} D1 = \sum_{n=0}^{N} \sum_{n'=0}^{N} d_{N,n}\ d_{N,n'}\ A_{n,n'} \ , \\ D2 = \sum_{n=0}^{N-1} \sum_{n'=0}^{N} d_{N-1,n}\ d_{N,n'}\ A_{n,n'} \ , \\ D3 = \sum_{n=0}^{N-1} \sum_{n'=0}^{N-1} d_{N-1,n}\ d_{N-1,n'}\ A_{n,n'} \ . \end{cases}$$

And similarly for the denominator

$$\mathcal{F}_\nu^{\mathrm{DEN}} = \alpha^2 \left(E1 - 2E2 + E3\right) + 2\alpha \left(E2 - E3\right) + E3 \,,$$

with

$$\begin{cases} E1 = \sum_{n=0}^{N} \sum_{n'=0}^{N} d_{N,n}\ d_{N,n'}\ B_{n,n'} \ , \\ E2 = \sum_{n=0}^{N-1} \sum_{n'=0}^{N} d_{N-1,n}\ d_{N,n'}\ B_{n,n'} \ , \\ E3 = \sum_{n=0}^{N-1} \sum_{n'=0}^{N-1} d_{N-1,n}\ d_{N-1,n'}\ B_{n,n'} \ . \end{cases}$$

Finally, this leads to the following rational function

$$\mathcal{F}_\nu = \frac{\alpha^2 \left(D1 - 2\,D2 + D3\right) + \alpha \left(2\,D2 - 2\,D3\right) + D3}{\alpha^2 \left(E1 - 2\,E2 + E3\right) + \alpha \left(2\,E2 - 2\,E3\right) + E3} \ .$$

Again, this is a second order equation in α that is easily solved, and only the solution satisfying $0 \leq \alpha \leq 1$ is retained. The analytical solution for α is not reproduced here for brevity, but the resulting beampattern $\mathcal{Y}_\nu\left(\Theta\right)$ is presented in Fig. 4.

6. CARDIOID PATTERN

6.1 Discrete-order cardioid pattern

Cardioid patterns (also referred to as *in-phase*) are designed so as to suppress the signal in the opposite direction ($\Theta = \pm 180°$), while exhibiting a maximally flat response in that direction. The cardioid pattern weights are given by (Eqn. 3.91 in [14])

$$\forall n \leq N,\ d_{N,n} = 4\pi\, \frac{(N!)^2}{(N+n+1)!\,(N-n)!} \,,$$

and the corresponding beampattern response is written

$$\mathcal{Y}_N\left(\Theta\right) = \left(\frac{1+\cos\Theta}{2}\right)^N \ .$$

6.2 Fractional-order cardioid pattern

Recalling the interpolation equation Eqn. (2), $\forall \nu \in \mathbb{R} \cap \left[(N-1)\,,N\right]$, $\mathcal{Y}_\nu\left(\Theta\right) = \alpha\,\mathcal{Y}_N\left(\Theta\right) + (1-\alpha)\,\mathcal{Y}_{N-1}\left(\Theta\right)$, it is trivial to see that

$$\alpha = \frac{\mathcal{Y}_\nu\left(\Theta\right) - \mathcal{Y}_{N-1}\left(\Theta\right)}{\mathcal{Y}_N\left(\Theta\right) - \mathcal{Y}_{N-1}\left(\Theta\right)} \ .$$

This relation should hold for any angle Θ. Considering for instance $\Theta = \frac{\pi}{2}$, we straightforwardly find the solution

$$\alpha = 2 - 2^{N-\nu} \ .$$

Again, one can verify that such solution satisfies the boundary conditions

$$\begin{cases} \alpha = 0 \ \Leftrightarrow\ \nu = N-1 \ , \\ \alpha = 1 \ \Leftrightarrow\ \nu = N \ . \end{cases}$$

The resulting beampattern $\mathcal{Y}_\nu\left(\Theta\right)$ is presented in Fig. 5 for various values of ν.

These results can further be extended to a more general family of "cardioid-like" patterns in the form

$$\mathcal{Y}_N\left(\Theta\right) = \left(\beta\ +\ (1-\beta)\,\cos\Theta\right)^N \ ,$$

provided that $\beta \in \left[\frac{1}{2}\,,1\right[$. This particular case is examined in [13], and yields the following solution

$$\alpha = \frac{\beta^{\nu-N+1} - 1}{\beta - 1} \ .$$

7. MAX-RE PATTERN

7.1 Discrete-order max-r_E pattern

The max-r_E beampattern is designed to optimize the norm of the energy vector [14, 15]. Its properties are somewhat similar to super-cardioids. The beampattern weights are expressed by (Eqn. 3.89 in [14])

$$\forall n \leq N,\ d_{N,n} = \mathcal{P}_n\left(\mathrm{r}_E(N)\right) \ ,$$

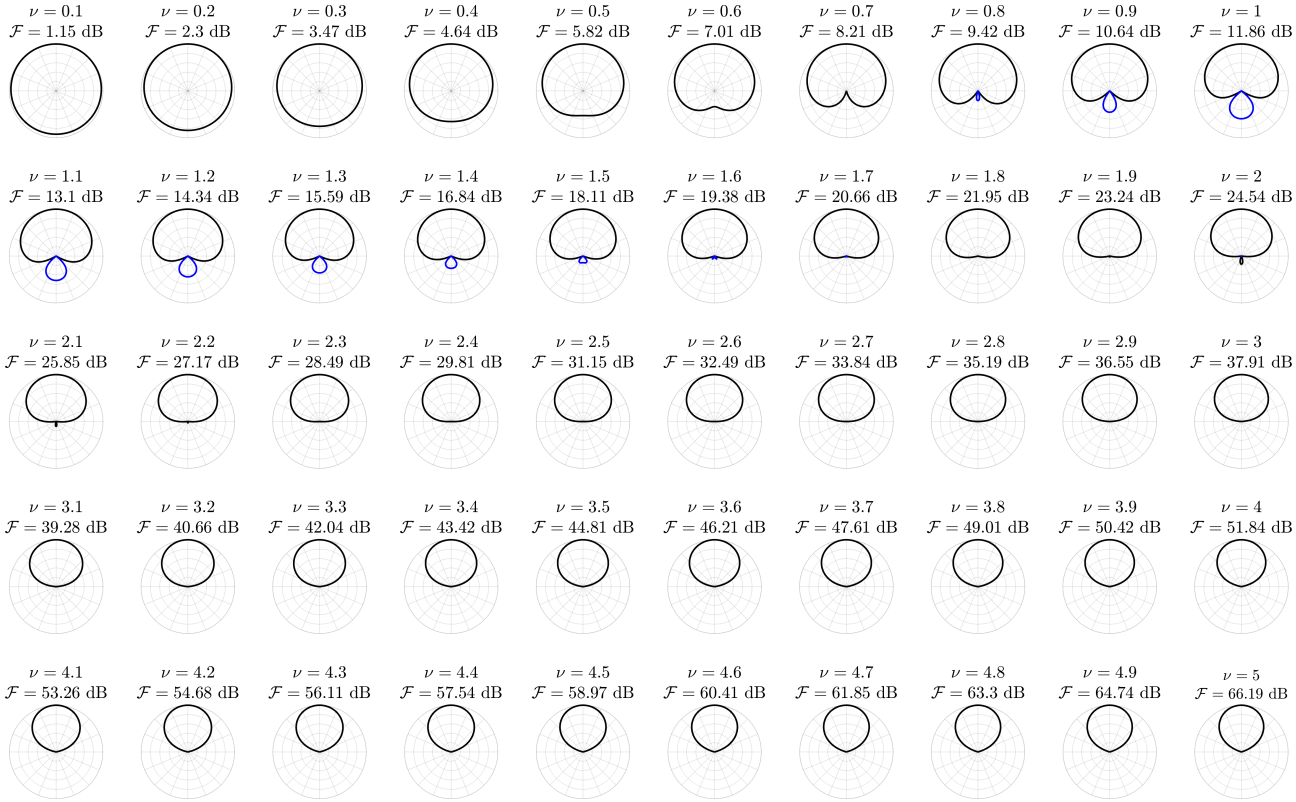

Figure 4: Fractional-order super-cardioid beampattern (the radial scale is logarithmic, with 6 dB/division).

where $\mathrm{r}_E(N)$ is the largest root of $\mathcal{P}_{N+1}(\cdot)$. According to Eqn. 10 in [15] , this can be approximated by

$$\mathrm{r}_E(N) \approx \cos\left(\frac{137.9^\circ}{N+1.52}\right) ,$$

as displayed in Fig. 6.

7.2 Fractional-order max-r_E pattern

Weights for the fractional-order max-r_E beampattern are trivially generalized to $\forall \nu \in \mathbb{R} \cap \left[(N-1), N\right]$

$$\forall n \leq N,\ d_{\nu,n} \approx \mathcal{P}_n\left(\cos\left(\frac{137.9^\circ}{\nu+1.52}\right)\right) ,$$

and the resulting polar response is displayed in Fig. 7.

8. CONCLUSION

In this article, we have derived simple analytic expressions for the design of spherical beampatterns with fractional orders. We have examined the most traditional beam shapes: hyper-cardioid, super-cardioid, cardioid, and max-r_E. In future work, we may extend the results to other design objectives, such as the Dolph-Chebyshev beampattern with constrained side lobe attenuation.

9. REFERENCES

[1] J. Meyer and G. Elko, "A highly scalable spherical microphone array based on an orthonormal decomposition of the soundfield," in *Proc. of the IEEE International Conference on Acoustics, Speech and Signal Processing (ICASSP)*, vol. 2, (Orlando, FL, USA), pp. II–1781–II–1784, IEEE, May 2002.

[2] G. W. Elko, "Differential Microphone Arrays," in *Audio Signal Processing for Next-Generation Multimedia Communication Systems* (Y. A. Huang and J. Benesty, eds.), pp. 11 – 65, Kluwer Academic Publishers, 2004.

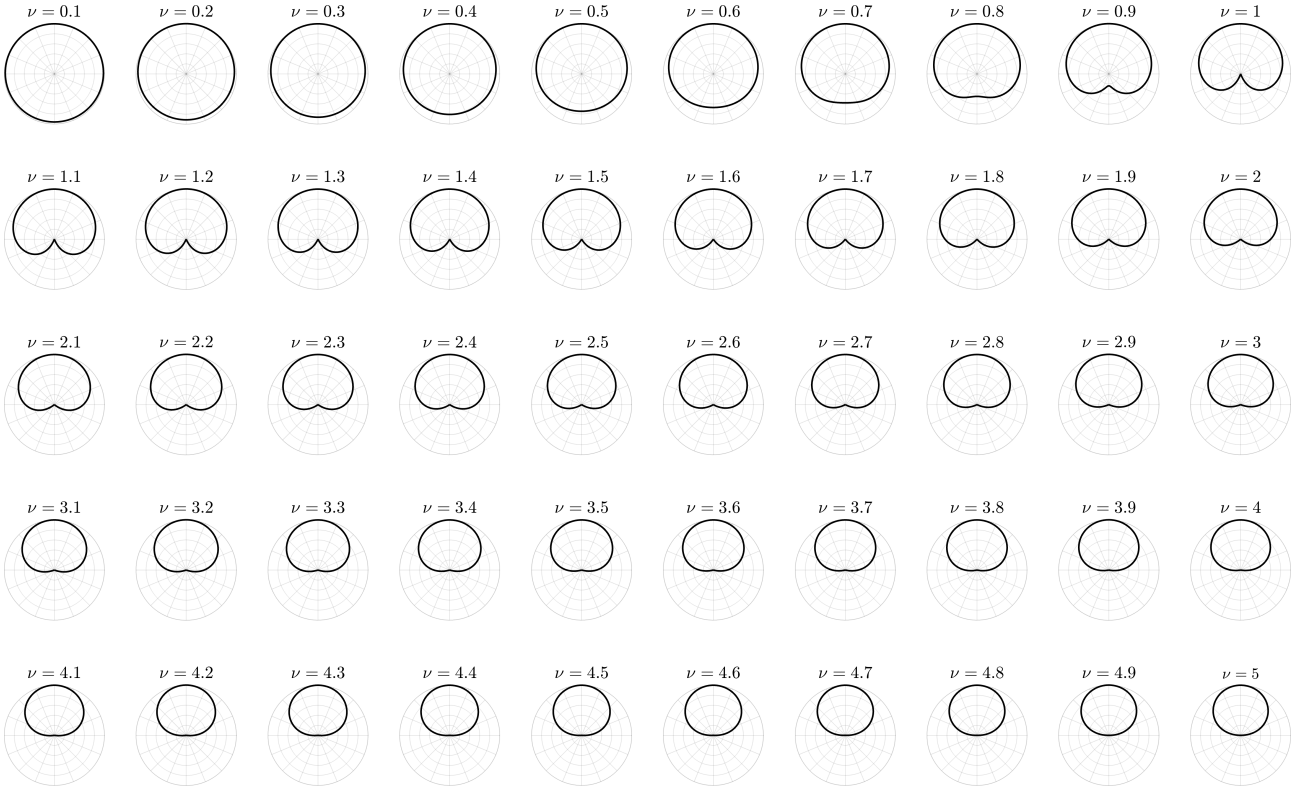

Figure 5: Fractional-order cardioid beampattern (the radial scale is logarithmic, with 6 dB/division).

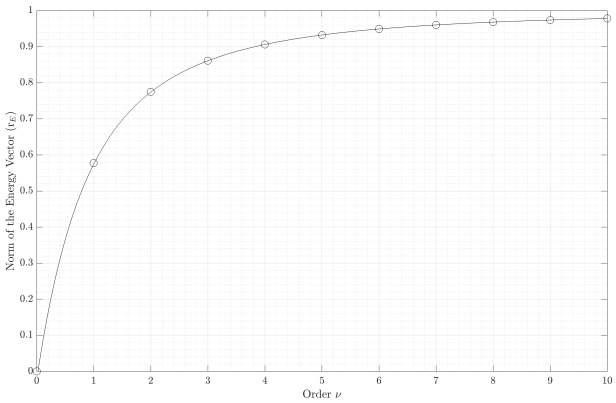

Figure 6: Norm of the energy vector for the max-r_E beampattern. Circle markers denote integer orders n; solid curve is for fractional-order ν.

[3] J. Meyer and G. W. Elko, "Spherical microphone arrays for 3d sound recording," in *Audio Signal Processing for Next-Generation Multimedia Communication Systems* (Y. Huang and J. Benesty, eds.), ch. 3, pp. 67 – 89, Kluwer, 2004.

[4] B. Rafaely, *Fundamentals of Spherical Array Processing – Second edition*. Springer-Verlag, 2019.

[5] J. Benesty, J. Chen, and I. Cohen, *Design of Circular Differential Microphone Arrays*, vol. 12. Springer Topics in Signal Processing, 2015.

[6] C. Pan, J. Benesty, and J. Chen, "Design of robust differential microphone arrays with orthogonal polynomials," *Journal of the Acoustical Society of America*, vol. 138, pp. 1079 – 1089, August 2015.

[7] D. P. Jarrett, E. A. P. Habets, and P. A. Naylor, *Theory and Applications of Spherical Microphone Array Processing*. Springer-Verlag, 2017.

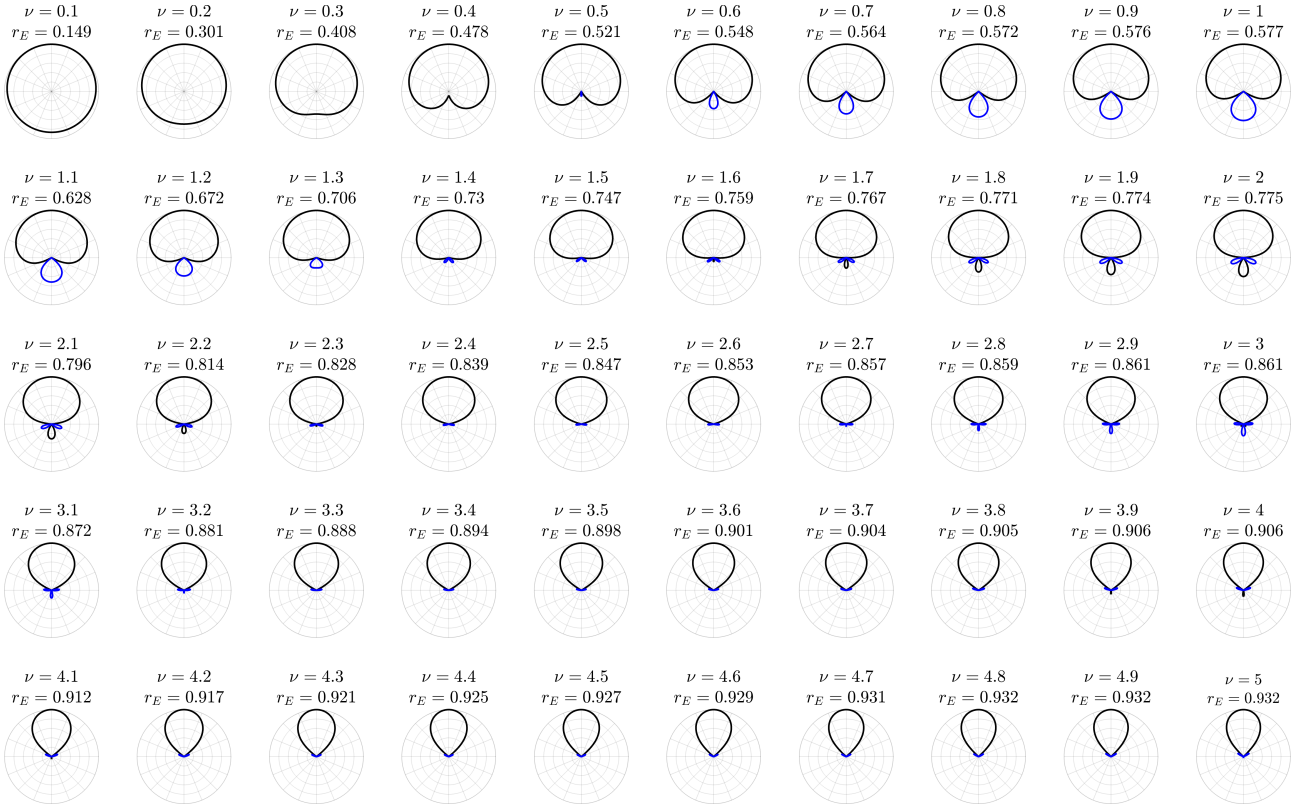

Figure 7: Fractional-order max-r_E beampattern (the radial scale is logarithmic, with 6 dB/division).

[8] L. Wang and J. Zhu, "Flexible Beampattern Design Algorithm for Spherical Microphone Arrays," *IEEE Access*, vol. 7, pp. 139488 – 139498, September 2019.

[9] E. D. Sena, H. Hachabiboglu, and Z. Cvetkovic, "A generalized design method for directivity patterns of spherical microphone arrays," in *Proc. of the IEEE International Conference on Acoustics, Speech and Signal Processing (ICASSP)*, (Prague, Czech Republic), pp. 125 – 128, May 2011.

[10] E. De Sena, H. Hacihabiboglu, and Z. Cvetkovic, "On the Design and Implementation of Higher Order Differential Microphones," *IEEE Transactions on Audio, Speech, and Language Processing*, vol. 20, pp. 162 – 174, June 2012.

[11] G. Huang, J. Chen, and J. Benesty, "A flexible high directivity beamformer with spherical microphone arrays," *Journal of the Acoustical Society of America*, vol. 143, pp. 3024 – 3035, May 2018.

[12] G. Huang, J. Chen, and J. Benesty, "Design of Planar Differential Microphone Arrays With Fractional Orders," *IEEE/ACM Transactions on Audio, Speech, and Language Processing*, vol. 28, pp. 116 – 130, October 2019.

[13] T. Carpentier, O. Warusfel, and J.-M. Jot, "Software Tools for Flexible Control of Radiation Synthesis," in *Proc. of the International Conference on Immersive and 3D Audio (I3DA)*, (Bologna, Italy), September 2023.

[14] J. Daniel, *Représentation de champs acoustiques, application à la transmission et à la reproduction de scènes sonores complexes dans un contexte multimédia*. PhD thesis, Université de Paris VI, 2001.

[15] F. Zotter and M. Frank, "All-Round Ambisonic Panning and Decoding," *Journal of the Audio Engineering Society*, vol. 60, pp. 807 – 820, October 2012.